THz Medical Imaging

Z. D. Taylor[1]; D. B. Bennett[2]; R. S. Singh[3]; P. Tewari [1]; N. Bajwa[1]; C. P. Kealey[3]; J. P. Hubschman[4]; E. R. Brown[5,6]; M. O. Culjat[1,3]; W. S. Grundfest[1,2,3]

[1]Dept. of Bioengineering, [2]Dept. of Electrical Engineering, [3]Dept. of Surgery, [4]Dept. of Ophthalmology, UCLA, Los Angeles, CA 90095, USA, [5]Department of Physics, [6]Department of Electrical Engineering, Wright State University, Dayton, OH 45435, USA

***Abstract*- This paper presents a pulsed, reflective THz imaging system operating at ~525 GHz center frequency with ~ 125 GHz of response normalized bandwidth and developed specifically for medical imaging applications. System parameters are discussed and the choice of effective operational bandwidth is motivated by hydration sensitivity calculations. Two promising medical applications of THz imaging are discussed: cornea and skin burns. For cornea, experimental data measuring the hydration of *ex vivo* porcine cornea under drying is presented along with intrinsic corneal hydration sensitivity calculations computed with spectroscopic measurements. For burns, images of 2nd degree, partial thickness burns were obtained in rat models *in vivo* over an 8 hour period. These images clearly show the formation and progression of edema in and around the burn wound area.**

I. Introduction

Terahertz illumination includes the millimeter and submillimeter-wavelength (3 mm to 0.033 mm) bands of the electromagnetic spectrum with frequencies between 100 GHz and 10 THz. The last decade has witnessed significant proliferation of THz devices and technologies with considerable attention devoted to medical imaging and diagnostics [1, 2]. THz medical imaging has been applied to the detection and spatial mapping of skin cancer [3], skin hydration [4], and breast cancer [5]. Recently THz imaging has been successfully applied to the imaging of burn wounds in *ex vivio* pig skin [6] and *ex vivo* corneal hydration [7]. These results detected local hydration changes due to burn temperatures and/or drying and have demonstrated possible clinical applications of THz imaging

In this paper we present an overview of a pulsed THz imaging system operating at a center frequency of 525 GHz and designed specifically for reflective medical imaging applications. A short discussion of system architecture is provided along with motivation on illumination frequency. These are followed experimental results and discussions of corneal and burn imaging; two very promising applications of THz medical imaging technology.

II. THz Imaging System

A. Design

A block diagram of the pulsed THz imaging system [4, 6-9] used to generate the images in this paper is shown in Figure 1. The THz source is a photoconductive switch [10, 11] pumped by a 780 nm femtosecond laser with a 230 fs pulse width, 20 MHz repetition rate, and ~ 8 mW of average power. At high bias fields (200 V/9 um gap ~ 222 kV/cm) the source produces an optical to quasioptical (THz) conversion efficiency of > 1% yielding average powers of up to 46 μW across 1 THz of bandwidth [11]. The switch is mounted on the backside of a high resistivity silicon hyperhemisphere and mounted ~ 60 mm away from a 76.2 mm effective focal length (EFL), 25.4 mm clear aperture OAP mirror thus matching photo conductive switch beam pattern and mirror numerical aperture (NA). The collimated beam is directed towards a 2nd OAP (50.8 mm EFL) where it is focused onto the target at a 14° angle forming a ~ 1 mm spot size. The reflected beam is collimated by a third parabolic mirror and then focused using a 25.4 mm (EFL) OAP into the feed horn of a 0-bias Schottky diode [12] detector mounted in a WR1.5 waveguide.

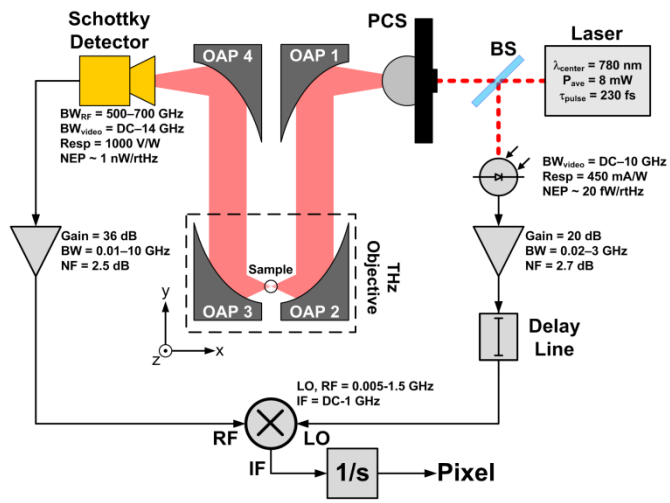

Fig 1: Block diagram of the THz imaging system. OAP directs THz illumination at 14° off the z-axis in the -x,-z direction.

Following the THz rectifier is a gated receiver consisting of a low-noise pulse amplifier, a double-balanced mixer, and a low pass filter (integrator). The rectified THz pulse is amplified (G = + 38 dB, BW = 10 GHz) and then coupled to the RF port of a double-balanced mixer. The gating is realized by driving the LO port of the mixer with a reference RF pulse generated from the mode-locked laser using a free space 99/1 beam splitter, photodiode and broadband amplifier. The reference pulse is passed through an RF delay line adjusted so that the pulse arrives at the mixer synchronous to the amplified THz pulse. The DC voltage from the IF port of the mixer is passed through a low pass filter, amplified with an audio frequency instrumentation amplifier and sampled using a 14 bit DAQ with a 1 ms time constant producing ~ 50 dB SNR.

Pixels are generated by raster scanning the target in the x and y directions, using stepper motors.

B. *Illumination Band*

The effective center frequency and bandwidth of the system are dictated by the pass band characteristics of the detector. An advantage of the waveguide mounting is that it provides well-defined pass bands with a sharp cut on frequency and a relatively sharp roll-off when the waveguide becomes over-moded.

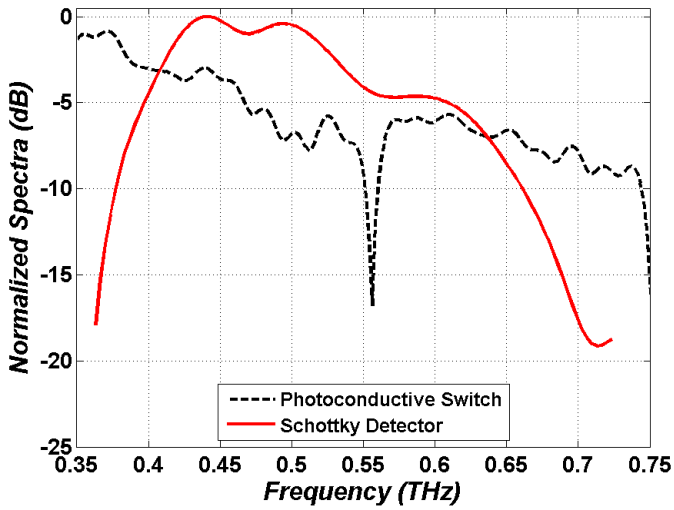

Fig 2: THz imaging system spectra. The dotted (black) line is the normalized photoconductive switch power spectral density. The water line was left in to reflect actual operation (non-evacuated). The solid line (red) is the Schottky diode normalized spectral responsivity. The response peaks at ~ 400 GHz and the total width reflects the operational band of a WR1.5 waveguide.

The normalized power spectral density of the photoconductive switch is displayed in Fig 2 superimposed on the normalized Schottky diode spectral responsivity. The switch spectrum was acquired with a Fourier Transform Infrared (FTIR) spectrometer and He-cooled composite bolometer. The detector spectral responsivity was measured with a THz photomixing setup [13].

$$f_c = \frac{\int_{\Omega_f} f\Re(f)S(f)df}{\int_{\Omega_f} \Re(f)S(f)df} \qquad \textbf{(1)}$$

$$\Delta f_c = \left(\frac{\int_{\Omega_f} f^2\Re(f)S(f)df}{\int_{\Omega_f} \Re(f)S(f)df} - f_c^2\right)^{1/2} \qquad \textbf{(2)}$$

The center frequency and response normalized bandwidth of the system are calculated using equations **(1)** and **(2)** where $\Re(f)$ is the detector spectral responsivity (red curve in Fig 2) and $S(f)$ is the switch power spectral density (black curve in Fig 2). These computations yield a center frequency of 525 GHz with 125 GHz of 3 dB bandwidth. This effective bandwidth in combination with 50.8 mm EFL mirrors provides diffraction limited spot size of ~ 1 mm and offers a sufficient tradeoff between hydration sensitivity and spatial resolution.

III. Hydration Sensitivity

For many THz medical imaging applications hydration is the dominant contrast mechanism and measurement sensitivity is determined by quantifying the expected change in THz tissue reflectivity for a given change in water volume fraction at a particular volume fraction. For this analysis we model tissue as a homogenous mixture of water and biological background which is described by a lossless dielectric of 4 [14]. The reflection coefficient of a half space of this tissue mixture in air is:

$$R(p_w, f) = \left(\frac{\sqrt{\varepsilon_0}cos(\theta_1) - \sqrt{\hat{\varepsilon}(p_w, f)}cos(\theta_2)}{\sqrt{\varepsilon_0}cos(\theta_1) + \sqrt{\hat{\varepsilon}(p_w, f)}cos(\theta_2)}\right) \qquad \textbf{(3)}$$

$$\hat{\varepsilon}\ s.t.\ \ p_w\left(\frac{\hat{\varepsilon} - \varepsilon_w}{\varepsilon_w + 2\hat{\varepsilon}}\right) + (1 - p_w)\left(\frac{\hat{\varepsilon} - \varepsilon_{BB}}{\varepsilon_{BB} + 2\hat{\varepsilon}}\right) = 0 \qquad \textbf{(4)}$$

where θ_1 and θ_2 are adjusted to reflect the polarization angle of incidence, $\hat{\varepsilon}$ is defined in equation **(4)**, ε_w is defined by the double debye model [15], ε_{BB} is the dielectric of the biological background, and the tissue half space is composed entirely of these two components Equation **(4)** is known as the Bruggeman model and is written here for a binary mixture. This model has been used previously to model the THz properties of tissues [7, 16]. The intrinsic sensitivity of THz imaging to hydration changes as a function of frequency is simply the derivative of equation **(3)** with respect to hydration:

$$\Re(p_w, f) = \frac{d}{dp}R(p_w, f) \qquad \textbf{(5)}$$

Further inspection of equations **(3)-(5)** reveals that at non-normal incidence the transverse-electric (TE) polarization will produce higher intrinsic contrast than the transverse-magnetic (TM) polarization. Thus equation **(3)** has been written for the TE case.

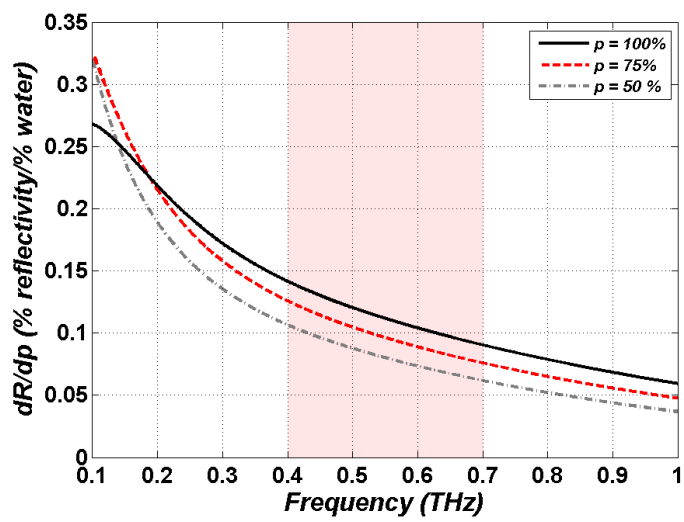

Fig 3: Intrinsic hydration sensitivity as a function of water concentration and illumination frequency assuming the validity of the double debye dielectric model and Bruggeman mixing theory.

Equation **(5)** has been simulated for hydration

concentrations of 100% (pure water), 75% (muscle tissue), and 50% (adipose tissue) and the trends are displayed in Fig 3. Not only does lower frequency illumination provide greater reflectivity, it also produces greater changes in reflectivity for a given change in water contrast with ~ 6 times more sensitivity at 100 GHz as compare to 1 THz. An interesting consequence of equation **(5)** is the crossover in delta reflectivity at ~ 150 GHz between pure water, and hydrated tissues. The highest intrinsic contrast available for hydration contrast in the physiologically relevant range at 100 GHz exceeds that of pure water, and one can envision building point measurement systems at millimeter wave frequencies if high resolution imaging is not required.

IV. Corneal Imaging

A. *Corneal Imaging Motivation*

The normal water content of the cornea is closely related to its transparency and refractive capabilities, and many diseases of the eye may measurably perturb it. Some, such as edema and corneal dystrophy, are diseases defined by the deterioration of the cornea's water-regulating process [17, 18]. The hydration of the cornea can also be perturbed by medical procedures such as LASIK or corneal graft surgery [19]. In LASIK, tissue ablation rates are strongly linked to corneal hydration and errors in the measurement of tissue hydration are often responsible for surgical overcorrection [20]. In corneal graft surgeries, immune rejection is preceded by the formation of edema and the reversibility of rejection events is inversely proportional to hydration [19].

Given the smooth surface of the cornea, its high water concentration by volume, and the near lossless properties of the collagen matrix, THz may be ideally suited to directly measure the hydration *in vivo,* thus providing a clinical tool capable of earlier detection and monitoring of corneal disease.

B. *Ex vivo Porcine Cornea*

Changes in hydration in *ex vivo* porcine corneas were visualized by monitoring *ex vivo* corneas undergoing drying. The loss of water from the stroma (interior bulk of the cornea) of these samples causes the cornea to deform significantly from its ideal spherical shape. To remove geometry variations from the experiment, the cornea was mounted in a flat geometry by pressing it against a thin quartz window using a porous foam material thus permitting evaporation from the side opposing the quartz (in-depth details of the experiment can be found in [7]). Images of a 2 cm x 3 cm area were acquired at 8 minute intervals over the course of 5 hours. The results from selected time instances corresponding to 87%, 84%, 79%, 75%, 70%, and 66% average water concentration are shown in Fig 4 with ~ 10 minutes elapsing between each image.

Each image is accompanied with its computed water concentration by volume calculated using sample mass measured between each image acquisition. Clear preferential drying from the outer edges is seen in the images, as the border closes further in towards the center with each subsequent frame. These edges suffer evaporative loss from the sides of the cornea in addition to losses from the epithelial (top) and endothelial (bottom) surfaces. The progression of drying from the outside-inward is the expected result due to the faster diffusion in the lateral directions relative to the thickness direction [21, 22]. This is also in agreement with observations from a previous preliminary study in which a single cornea was imaged at a one point in time without constraint to its geometry [23].

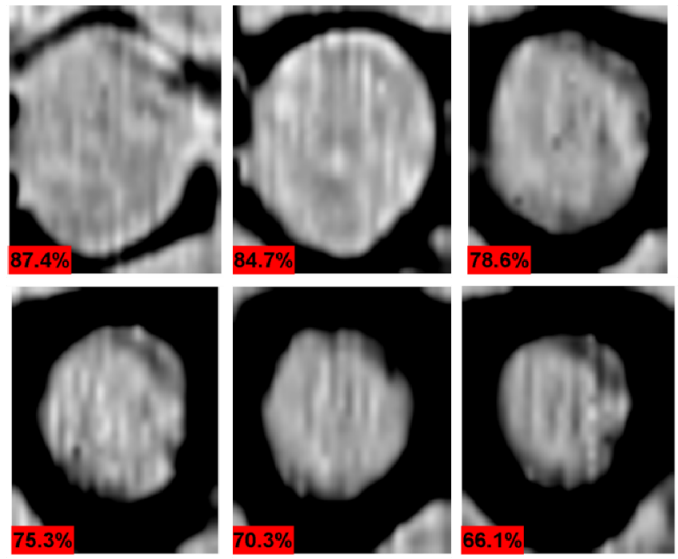

Fig 4: Time lapse imaging of drying cornea with hydration by volume percentages denoted in the bottom left corner of each image. Reprinted from [7]

C. *Corneal Spectroscopy and Hydration Sensitivity*

Following the corneal imaging experiments, spectroscopic measurements on *ex vivo* corneas were performed to confirm the role of hydration and illumination frequency in contrast generation. Nine corneas were soaked in a 0%, 3%, 5%, and 7% polyethylene glycol (PEG) solutions containing 0.15M NaCl for 3 days. The concentrations of these solutions produce different equilibrium water concentrations in the corneas that varied between 79.1% and 91.5%. The corneas were abutted to a 12.7 um thick Mylar film thus forcing it into a flat, orthogonal geometry with respect to the THz aperture. The incidence angle of the source was limited to 30 degrees by the optics of the Teraview time-domain system. Further details of this experiment can be found here [7].

The relationship between water concentration and THz reflectivity for 5 representative illumination frequencies is displayed in the inset at the top right corner of Figure 5. The trends from top to bottom are 0.25 THz (blue), 0.45 THz (red), 0.65 THz (cyan), 0.85 THz (magenta), and 1.05 THz (green) respectively. The x-axis is constrained to the physiologically relevant range of corneal hydration. These points were calculated using reflective spectra across 1 THz of bandwidth and display an approximate linear relationship between hydration and THz reflectivity. Superimposed on the data sets are least-squares fit lines. These fits display a decreasing slope as the frequency increases. The slope of each line is in units

of % reflectivity/% hydration and describes the intrinsic sensitivity of THz imaging to corneal hydration.

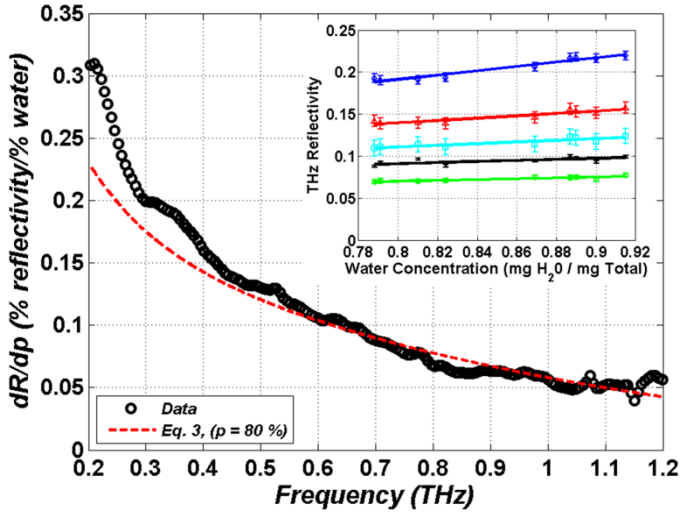

Fig 5: Time lapse imaging of drying cornea with hydration by volume percentages denoted in the bottom left corner of each image. The data trace was reprinted from [7].

The % reflectivity/% hydration slope at each frequency point computed with the spectra of all 9 cornea is displayed in Figure 5 and confirms a monotonically decreasing intrinsic hydration sensitivity as a function of increasing illumination frequency. Equation **(3)** was simulated for p = 0.8 and θ_i = 30° and the computation (read dotted line) is superimposed on the data in Figure 5. The fit between simulation and data is quite good at the upper frequencies and degrades a bit at the lower frequencies which we attribute to alignment problems in the spectrometer during the experiment.

These results in addition to recently published data [7] suggest that reflective THz imaging can be successfully applied to cornea using water as the dominant contrast mechanism and may provide hydration sensitivity superior to other ophthalmologic diagnostic systems. They also confirm that Debye and Bruggeman theory accurate model THz/corneal tissue interactions.

V. Burn Imaging

A. *Burn Imaging Motivation*

Approximately 500,000 patients are treated for burns in the United States annually and of these, ~50,000 require hospitalization, and 400 die each year, making mortality from burns the fifth leading cause of injury-related death in the United States [24]. In addition to their high mortality, large burns are also very morbid, requiring extensive treatment and rehabilitation regimens. It has been estimated that costs related to treatment of burn injuries account for 13% of all medical claims despite their relatively low incidence [25].

The crux of burn wound assessment is distinguishing between superficial and deep partial thickness burns. This is because deep partial thickness burns and full thickness burns require skin grafting, whereas more superficial burns can be managed conservatively [26]. Currently, the most commonly used methods for estimating burn depth are visual and tactile assessment. These methods are highly inaccurate, however, because there is a lag time of 3-5 days before a burn's gross appearance reflects the true extent of injury [27]. Additionally, this method lacks standardization because it relies entirely on the experience of the surgeon.

The physiological response of tissue to a burn injury is the formation and maintenance of edema. THz imaging is very sensitive to these fluid shifts and spatial and temporal characterization of edematous tissue may improve the accuracy of burn depth estimation.

B. *In vivo Burn Imaging results*

Initial in vivo burn images were acquired with rats as they are the most practical animals on which to perform feasibility studies (in-depth details of the experiment can be found in [28]). The study was approved by the UCLA Institutional Review Board (#2009-094-02). Two male Sprague Dawley rats weighing 200-300g were anesthetized with isofluorane (an analgesic) prior to burn. The combination of substances and their delivery technique was chosen to minimize any physiological activity that would affect the immune response to the applied burn. A flat 4 cm x 4 cm area on the both abdomens was shaved with electric clippers to minimize irritation and then cleaned with antiseptics to reduce the chance of infection. The rats were then placed beneath the imaging system and the shaved area of the abdomen flattened with a 12.7 um thick circular mylar window positioned against the skin with light pressure.

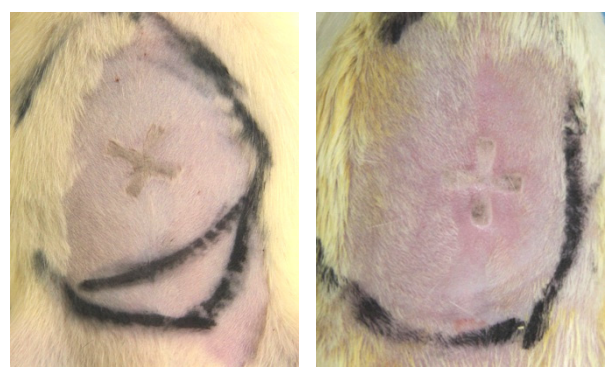

Fig 6: THz in vivo wounds. (Left) Rat abdomen burn of experiment 1. (Right) Rat abdomen burn of experiment 2. Left image reprinted from [29]

A '+' shaped burn was inflicted using a brass brand within the control scan area. The '+' profile brand measured 15 mm x 15 mm with 3 mm thick arms. The brand was heated to ~ 220° C using a hot plate and pressed against the skin with contact pressure for ~ 10 seconds. Following application of the burn the Mylar window was placed back over the burned region and the injury was re-imaged. THz burn images were acquired every 15-30 min for the next 8 hr with the Mylar window removed between each image acquisition to allow the responses to progress naturally. Images of the burn wounds immediately following branding for both rats are displayed in Figure 6; the image on the left corresponds to experiment 1 and the image on the right corresponds to experiment 2

A THz image of a 35 mm diameter area of unburned skin beneath the Mylar window for experiment 1 is displayed in the top left of Fig 7. The Mylar window flattens the imaging field but is extremely thin so the varying surface profile of the rat belly is still visible. The Mylar window frame is made of steel and reflects a larger portion of THz illumination than the skin thus the circular field of view is bounded by a white (highly reflecting area).

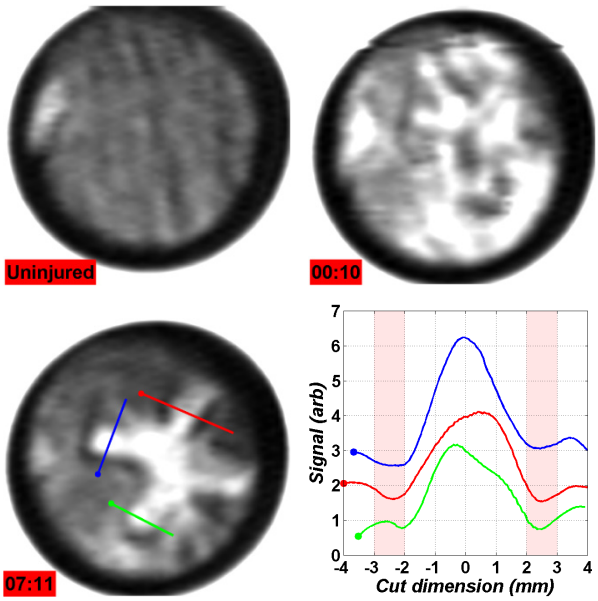

Fig 7: THz in vivo burn images. (Top Left) Rat abdomen prior to application of heated brand. (Top Right) rat abdomen 10 min post burn. (Bottom Left) >1 hour post burn, (Bottom Left) burn injury after > 7 hours. (Bottom Right) Cuts through the image. (color online)

The immune response of skin tissue immediately following a burn is characterized by a rush fluid to the sight of injury resulting in both the burn and surrounding area to becoming edematous. The image at the top right of Fig 7 shows an acute influx of H_2O throughout the region with non-burned areas reflecting as much incident THz radiation as burned areas. After 7, hours the edema has localized completely to the brand contact area and the surrounding skin has returned to normal, non-burned reflectivity. Additionally a dark, low reflectivity ring of tissue is seen along the periphery of the hyperhydrated brand contact area. A trace of pixel amplitudes across thee of the arms on the '+' shaped burn is plotted in the bottom right of Fig 7 where each color corresponds to cut trajectory in the image of the bottom right of Fig 7. Each trace has been given a different offset for clarity. All three cuts display a dip in reflectivity on either side of the peak.

Burn wound pathophysiology is divided into three concentric regions: the zones of coagulation, stasis, and hyperemia [30]. The zone of coagulation (hyperperfused) is at the center of the burn and contains irreversibly damaged cells, denatured protein, and edema. The zone of stasis surrounds the zone of coagulation and contains hypoperfused tissue. The zone of hyperemia forms the outer ring and is characterized by edematous, hyperperfused tissues. Ancillary with the appearance of these three zones are large fluid shifts both locally and systemically. Investigations into these fluid shifts have concluded that local water concentration can increase by as much as 80% within 10 minutes of injury, and that this response is proportional to the depth of injury [31, 32].

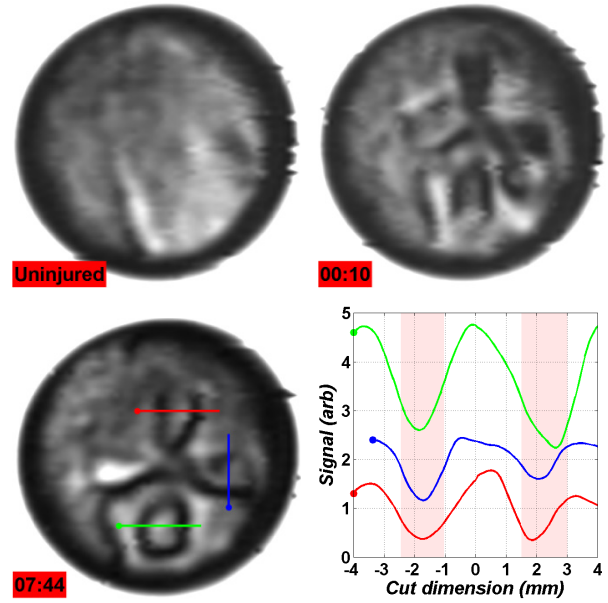

Fig 8: THz in vivo burn images. (Top Left) Rat abdomen prior to application of heated brand. (Top Right) rat abdomen 10 min post burn. (Bottom Left) >1 hour post burn, (Bottom Left) burn injury after > 7 hours. (Bottom Right) Cuts through the image. (color online)

The poorly reflecting boundary around the burn injury is hypoperfused skin its estimated extent is highlighted with light red regions in the plot on the bottom left of Fig 7. Given the location of these dips they are believed to be the zone of stasis. To our knowledge, this represents the first time that the zone of stasis has been imaged with any imaging modality.

The results of experiment 2 are displayed in Fig 8 using the exact same drug and burn protocol as experiment 1. The unburned image bears significant resemblance to experiment 1 with slightly higher peak reflectivity but nearly identical average reflectivity. The THz image immediately following the burn (top right of Fig 8) however displays a marked difference in hydration/reflectivity profile. There are areas of slightly increased profusion but the dominant factor is the low reflecting (hypoperfused) tissue in the brand contact area. This is the opposite effect observed in experiment 1 but similar to *ex vivo* results reported in the literature [6]. At 7 hours, 3 of the '+' brand arms have returned to normal reflectivity suggesting the lack of a coagulation zone. However, there are deep, thick hypoperfused rings around each burn suggesting a very pronounced zone of stasis.

Cuts through three of the '+' burn arms are displayed in the bottom right of Fig 8 and confirm the lack of response from the zone of coagulation as well as the large dips in THz reflectivity corresponding to the zone of stasis. Although the burn protocol was exactly the same between the rats and the visible image of the burns was similar, the THz reflectivity of the

zones of coagulation and zone of stasis from these 2 experiments was markedly different. A histology protocol is currently underway to explore the possible influence of physiological variation and other factors to the THz image.

CONCLUSIONS

A reflective THz medical imaging system operating at 525 GHz with 125 GHz of 3 dB bandwidth was presented. The system uses a radar inspired receiver architecture to generate reflectivity maps of physiological tissue based on gradients in water concentration. The center frequency of 525 GHz has been determined theoretically and experimentally to be a sufficient tradeoff between spatial resolution and intrinsic hydration sensitivity.

Two promising medical imaging applications of THz were presented: corneal hydration sensing, and burn wound imaging. An image set of an ex vivo porcine cornea under drying was presented suggests that water is the dominant contrast mechanism in THz corneal imaging. Additionally, the intrinsic hydration sensitivity of THz imaging to cornea was computed using spectroscopic measurements and fit to a model employing double debye theory and Bruggeman mixing theory thus confirming water as the dominant contrast mechanism.

Imagery of *in vivo* burns obtained on rat models were presented for 2 specimens. The first experiment displayed significant edema in zone of coagulation while second experiment showed almost a complete lack of edema. clear zones of stasis were observed in both experiments however the zones were much more pronounced in experiment 2.

REFERENCES

[1] P. H. Siegel, "Terahertz technology in biology and medicine," *Microwave Theory and Techniques, IEEE Transactions on,* vol. 52, pp. 2438-2447, 2004.

[2] P. H. Siegel, "Terahertz technology," *Microwave Theory and Techniques, IEEE Transactions on,* vol. 50, pp. 910-928, 2002.

[3] R. M. Woodward, B. Cole, V. P. Wallace, D. D. Arnone, R. Pye, E. H. Linfield, M. Pepper, and A. G. Davies, "Terahertz pulse imaging of in-vitro basal cell carcinoma samples," in *Lasers and Electro-Optics, 2001. CLEO '01. Technical Digest. Summaries of papers presented at the Conference on*, 2001, pp. 329-330.

[4] R. S. Singh, Z. D. Taylor, P. Tewari, D. Bennett, M. O. Culjat, H. Lee, E. R. Brown, and W. S. Grundfest, "THz imaging of skin hydration: motivation for the frequency band," San Francisco, California, USA, 2010, pp. 755513-8.

[5] A. J. Fitzgerald, V. P. Wallace, M. Jimenez-Linan, L. Bobrow, R. J. Pye, A. D. Purushotham, and D. D. Arnone, "Terahertz Pulsed Imaging of Human Breast Tumors1," *Radiology,* vol. 239, pp. 533-540, May 2006 2006.

[6] Z. D. Taylor, R. S. Singh, M. O. Culjat, J. Y. Suen, W. S. Grundfest, H. Lee, and E. R. Brown, "Reflective terahertz imaging of porcine skin burns," *Opt. Lett.,* vol. 33, pp. 1258-1260, 2008.

[7] Z. D. T. D. B. Bennett, D. Sassoon, P. Tewari, R. D. Johnson, R. Singh, M. O. Culjat, J.-P. Hubschman W. S. Grundfest, "Terahertz sensing in corneal tissues," *accepted, J Biomed Optics, 2010.*

[8] Z. D. T. D. B. Bennett, S. Sung, N. Bajwa, B. Makkabi, R. S. Singh, P. Tewari, M. O. Culjat, W. S. Grundfest, E. R. Brown, "Terahertz time-lapse video of hydration in physiological tissues," presented at the SPIE BiOS, San Fransisco, CA.

[9] Z. D. Taylor, R. S. Singh, M. O. Culjat, J. Y. Suen, W. S. Grundfest, and E. R. Brown, "THz imaging based on water-concentration contrast," Orlando, FL, USA, 2008, pp. 69490D-8.

[10] J. Y. Suen, W. Li, Z. D. Taylor, and E. R. Brown, "Characterization and modeling of a terahertz photoconductive switch," *Applied Physics Letters,* vol. 96, pp. 141103-141103-3, 2010.

[11] Z. D. Taylor, E. R. Brown, J. E. Bjarnason, M. P. Hanson, and A. C. Gossard, "Resonant-optical-cavity photoconductive switch with 0.5% conversion efficiency and 1.0W peak power," *Opt. Lett.,* vol. 31, pp. 1729-1731, 2006.

[12] http://vadiodes.com/

[13] J. E. Bjarnason, E. R. Brown, and T. M. Korter, "Comparison of the THz absorption feature in lactose to related saccharides," Orlando, FL, USA, 2007, pp. 65490L-9.

[14] A. J. F. Elizabeth Berry, Nickolay N. Zinov'ev, Gillian C. Walker, Shervanthi Homer-Vanniasinkam, Caroline D. Sudworth, Robert E. Miles, J. Martyn Chamberlain, Michael A. Smith, "Optical properties of tissue measured using terahertz pulsed imaging," in *Proceedings of SPIE: Medical Imaging*, 2003, pp. 459-470.

[15] J. Xu, K. W. Plaxco, S. J. Allen, J. E. Bjarnason, and E. R. Brown, "0.15-3.72 THz absorption of aqueous salts and saline solutions," *Applied Physics Letters,* vol. 90, pp. 031908-031908-3, 2007.

[16] D. B. Bennett, W. Li, Z. D. Taylor, W. S. Grundfest, and E. R. Brown, "Stratified Media Model for Terahertz Reflectometry of the Skin," *accepted, IEEE Sensors Journal,* 2010.

[17] A. P. Adamis, V. Filatov, B. J. Tripathi, and R. A. m. C. Tripathi, "Fuchs' endothelial dystrophy of the cornea," *Survey of Ophthalmology,* vol. 38, pp. 149-168, 1993/10// 1993.

[18] G. Klintworth, "Corneal dystrophies," *Orphanet Journal of Rare Diseases,* vol. 4, p. 7, 2009.

[19] V. M. Borderie, O. Touzeau, T. Bourcier, C. e. Allouch, E. Zito, and L. Laroche, "Outcome of Graft Central Thickness After Penetrating Keratoplasty," *Ophthalmology,* vol. 112, pp. 626-633, 2005.

[20] P. J. Dougherty, K. L. Wellish, and R. K. Maloney, "Excimer laser ablation rate and corneal hydration," *Am J Ophthalmol,* vol. 118, pp. 169-76, Aug 15 1994.

[21] B. A. Holden, J. J. Mcnally, and P. Egan, "Limited lateral spread of stromal edema in the human cornea fitted with a ('donut') contact lens with a large central aperture," *Curr Eye Res,* vol. 7, pp. 601-605, 1988.

[22] B. O. Hedbys and S. Mishima, "Flow of water in the corneal stroma," *Exp Eye Res,* vol. 1, pp. 262-75, Mar 1962.

[23] R. S. Singh, P. Tewari, J. L. Bourges, J. P. Hubschman, D. B. Bennett, Z. D. Taylor, H. Lee, E. R. Brown, W. S. Grundfest, and M. O. Culjat, "Terahertz sensing of corneal hydration," in *32nd Annu Int Conf IEEE Eng Med Biol Soc*, Buenos Aires, 2010.

[24] American Burn Association (ABA), Burn incidence and treatment in the US: 2007 fact sheet

[25] American Burn Association (ABA) National Burn Repository (2005 Report)

[26] A. D. Jaskille, J. W. Shupp, M. H. Jordan, and J. C. Jeng, "Critical Review of Burn Depth Assessment Techniques: Part I. Historical Review," *Journal of Burn Care & Research,* vol. 30, pp. 937-947 10.1097/BCR.0b013e3181c07f21, 2009.

[27] V. Singh, L. Devgan, S. Bhat, and S. M. Milner, "The Pathogenesis of Burn Wound Conversion," *Annals of Plastic Surgery,* vol. 59, pp. 109-115 10.1097/01.sap.0000252065.90759.e6, 2007.

[28] Tewari et. al. "THz imaging of In vivo Burn wounds" In review, Optics Letters

[29] Tewari et. al. "THz imaging of In vivo Burn wounds" In review, Optics Letters

[30] D. M. Jackson, "The diagnosis of the depth of burning," *British Journal of Surgery,* vol. 40, pp. 588-596, 1953.

[31] G. D. Warden, "Burn shock resuscitation," *World Journal of Surgery,* vol. 16, pp. 16-23, 1992.

[32] E. Reiss, J. A. Stirman, C. P. Artz, J. H. Davis, and W. H. Amspacher, "Fluid and Electrolyte Balance in Burns," *Journal of the American Medical Association,* vol. 152, pp. 1309-1313, August 1, 1953 1953.